J Nanostruct 13(3): 755-768, Summer 2023

RESEARCH PAPER

Response Surface Optimization of Removal of Rhodamine B Dye Using a Synthesized Ni-Based Metal-Organic Framework Adsorbent

Bahie Mohammadi [1], Tahereh Momeni Isfahani [1], Farnaz Maghazeii [2]*

[1] Department of Chemistry, Faculty of Science, Arak Branch, Islamic Azad University, Arak, Iran

[2] Department of Physics, Faculty of Science, Arak Branch, Islamic Azad University, Arak, Iran

ARTICLE INFO

Article History:
Received 19 March 2023
Accepted 27 May 2023
Published 01 July 2023

Keywords:
Experimental design
Metal- organic framework
Removal
Rhodamine B

ABSTRACT

In this research, removal of Rhodamine B (RB) dye from aqueous samples was investigated by a new Ni (II) based metal-organic framework (MOF) synthesized named [Ni(II) L]n [where L= 4, 4′-diamino diphenyl sulfone] (Ni- MOF). These materials were fully characterized using Fourier transform infrared (FT-IR), field emission scanning electron microscopy (FESEM), energy-dispersive X-ray spectroscopy (EDX), TGA/DTG and X-ray diffraction (XRD). WE used response surface methodology (RSM) based on the central composite design (CCD) to study the effects of four various parameters including dye concentration, MOF dosage, contact time and pH on the process of adsorption. The optimal condition for removal of RB was achieved for pH=9, 0.063 g of MOF for 25 mL of 16.06 mg/lit dye concentration and contact time of 39 minutes. Adsorption equilibrium and kinetic data were fitted with the Langmuir monolayer isotherm model (q_{max}=163.66 mg/g and R^2= 0.9827) and like pseudo second-order kinetics mechanism (R^2=0.992).

How to cite this article
Mohammadi B., Momeni Isfahani T., Maghazeii F. Response Surface Optimization of Removal of Rhodamine B Dye Using a Synthesized Ni-Based Metal-Organic Framework Adsorbent. J Nanostruct, 2023; 13(3):755-768. DOI: 10.22052/JNS.2023.03.016

INTRODUCTION

In today's life, the lack of safe water is one of the main problems of human societies, so there's no wonder that treatment of toxic and nontoxic pollutants from the water resource has become of great importance.

[1]. Synthetic dyes are one of the major reasons of water pollution, that not only lessen the transparency of water bodies in the aquatic system, but also influences human health directly or indirectly [1, 2]. It is stated that more than 100,000 commercial dyes are produced every year and poured into wastewater without purification [3]. Rhodamine B (RB) a widely administered dye in food industries, biological staining, and biomedical laboratories, accounts as a the most substantial water-soluble organic dye, [4]. Because of the cancerous nature of RB, the administration of RB has been omitted in food industries for years. But, along with the development of industry and the illegal depletion, RB still has administered food supplies encountering to human health risk. Therewith, the removal of dye from liquid waste is of topmost emphasis prior to entering in water flow and impact on environment. [5]. Different physical and chemical techniques of

* Corresponding Author Email: ta.momeni@iau.ac.ir

color removal from aqueous solution include methods like electrolysis [6], flocculation [7], chemical oxidation [8], and adsorption [9-11] have been utilized by researchers [12]. Also lately, sophisticated equipment involving photochemical, electrochemistry, chromatographic, etc. has been applied [13]. The adsorption method is the most extensively utilized high impressive, low-cost technique to dye removal from water. Different adsorption materials like commercial active carbon, metal- organic framework natural materials, and bio adsorbents have been utilized for dye adsorption processes [14-17].

Mmetal-organic frameworks (MOFs) consider as a crystalline porous material that are famous for their different applications. MOFs have a topmost application, gaining the interest of researches for having a simple synthesis method. Layering of solutions, solvent evaporation reactants,or slow diffusion are the most applicable synthesis method[18-24]. MOFs are preferable porous materials due to their high/tunable porosity, nanoscale porosity, large surface area, variant structures pore functionality, diverse pore architectures/compositions, free metal sites, and etc. There have a broad application, primary for removal, separation, and adsorption-based determination processes. So, lately, some studies have been focused on the adsorption/separation properties of different pollutants with MOFs [16, 25-27].

Different methods are available for process optimization. Response surface methodology (RSM) are prosperous approaches for process optimization. These two mentioned methods increase the efficiency of process, depletion the number of unnecessary parameters in the process, contributing to lower operation cost and more fast experimental studies [28]. RSM is a collection of experimental design techniques modeling the experiment using mathematical and statistical methods grading the impact of some parameters, and obtaining the preferential conditions for an optimal response using a minimum number of experiments. RSM illustrates the relevence of various independent factors with one or more responses. The goal of RSM method is to get the favorable response and discovering the variation of response in a given direction using adjustment of the design factors [29].

There was not any report for the dye degradation efficiency of Ni (II) based metal-organic framework (MOF) adsorbent. In this study, removal of Rhodamine B (RB) dye from aqueous samples by a new Ni (II)- MOF synthesized named [Ni (II) L] n [where L= 4, 4´-diamino diphenyl sulfones (DAP)] was studied. The influence of parameters like pH of the solution, primary concentration of dye, a dosage of MOF, and contact time were evaluated by central composite design (CCD; 5 levels and 4 factors) using RSM. However, this study observed that Ni-MOF can be considered as a catalyst [30].

MATERIALS AND METHODS

Materials and instruments

Chemicals including Rhodamine B (RB), HCl, NaOH, 4, 4´-diamino diphenyl sulfone (DAP) and Ni $(NO_3)_2 6H_2O$ were purchased from Sigma-Aldrich. One gram of RB was dissolved in 1000 ml double distilled water as the stock solution (1000 ppm) of Rhodamine B and working solution with desired concentration was obtained from dilution of stock solution. First, the Ni (II)- MOF was synthesized and in the second step it characterized by FT-IR, FESEM, EDX and XRD. The field emission scanning electron microscopy (FE-SEM; Philips, XL30, Netherland) was applied for morphological study of MOF. An automated diffractometer with Cu K_α radiation (ASENWARE AW-XDM300, 40KV) was applied for X-ray diffraction (XRD) pattern. FT-IR spectrophotometer (Perkin ELMER) was applied to record the absorbent of material using Fourier transform infrared spectroscopy. The RB concentration was determined with Agilent UV/Vis 8453 spectrophotometer at wavelength of 542 nm. The experimental design analysis was performed using the design expert software version 7.0.0 Trial.

Preparation of organic-metal framework of nickel particles

The MOF was prepared via a solvent evaporation method [31]. The molar ratio of DAP ligand to $Ni(NO_3)_2 6H_2O$ for the synthesis of MOF of nickel particles was mmol. first, DAP dissolve in methanol at room temperature and stirred by magnetic stirrer for 10 minutes, then the solution of $Ni(NO_3)_2 6H_2O$ was added to it . Obtained solution stirred and then NaOH solution(10%) was added dropwise. The final solution was stirred for 60 to 80 min and it was heated for 20 min in 50 ^{0}C. Finally, the filtered solution was rinsed with methanol to make a pure deposition and allowed to evaporate for several days[30].

Adsorption experiments

The adsorption of RB onto MOF in removal was studied in batch experiments. Four successive run performed in a fixed time interval according to the experimental design pattern. Filtration method utilized for extracting of MOF and RB concentration in the supernatant determined using UV-Vis spectrophotometer. The calibration of the RB concentration according to the Beer-Lambert law at the maximum wavelength of 542 nm. Removal percentage(%R) and equilibrium adsorption of the RB by MOF from the aqueous solution were calculated using the following equations respectively [32]:

$$\%R = \frac{C_0 - C_e}{C_0} \times 100 \quad (1)$$

$$Q_e = \frac{C_0 - C_e}{W} \times V \quad (2)$$

Where C_0 and C_e are the first and equilibrium concentrations of the RB in mg L^{-1}, Q_e is the equilibrium adsorption capacity of RB at C_e (mg g^{-1}), V is the volume of the solution (L) and w is the mass of MOF (g).

Experimental design and statistical analysis

Response Surface (RSM) methods utilized for optimization of the relation between four factors and their responses. The second order model focusing on removal process performed using public optimization model of RSM and Central Composite Design (CCD), [3, 33]. In the

Table I. Central Composite Design Parameters Obtained for different Runs, Experimental Values of four Variables, and Responses for the Adsorption of RB by Ni-MOF.

Factors	levels				
	-α	-1	0	+1	+α
A: pH	3.00	5.00	7.00	9.00	11.00
B: RB Concentration (mg L^{-1})	5.00	10.00	15.00	20.00	25.00
C: Ni- MOF dose (g)	0.020	0.035	0.050	0.065	0.080
D: contact time (min)	10.00	20.00	30.00	40.00	50.00

Run	Factors				% Removal	
	A	B(mg L^{-1})	C(g)	D(min)	Predicted	Experimental
1	11.00	15.00	0.050	30.00	78.98	79.75
2	9.00	20.00	0.065	40.00	99.05	99.81
3	5.00	10.00	0.065	20.00	45.74	44.83
4	7.00	5.00	0.050	30.00	89.57	90.56
5	3.00	15.00	0.050	30.00	14.29	14.24
6	9.00	10.00	0.065	20.00	83.04	82.48
7	9.00	10.00	0.035	40.00	94.59	93.16
8	7.00	15.00	0.050	50.00	92.17	91.98
9	7.00	15.00	0.020	30.00	79.89	80.17
10	5.00	20.00	0.065	40.00	80.95	79.91
11	9.00	20.00	0.035	20.00	80.80	80.85
12	9.00	20.00	0.065	20.00	83.02	81.62
13	7.00	15.00	0.050	30.00	90.87	90.26
14	7.00	15.00	0.080	30.00	88.51	88.94
15	7.00	15.00	0.050	30.00	90.57	90.26
16	5.00	20.00	0.065	20.00	39.97	41.5
17	7.00	15.00	0.050	10.00	52.45	53.36
18	9.00	20.00	0.035	40.00	88.41	88.52
19	7.00	15.00	0.050	30.00	89.90	90.26
20	9.00	10.00	0.035	20.00	92.71	92.95
21	7.00	15.00	0.050	30.00	89.01	90.26
22	5.00	10.00	0.035	40.00	67.16	67.76
23	7.00	15.00	0.050	30.00	90.48	90.26
24	5.00	10.00	0.035	20.00	48.02	47.34
25	5.00	20.00	0.035	20.00	33.59	32.79
26	7.00	25.00	0.050	30.00	82.87	82.59
27	9.00	10.00	0.065	40.00	93.22	93.22
28	5.00	20.00	0.035	40.00	60.02	60.66
29	7.00	15.00	0.050	30.00	90.68	90.26
30	5.00	10.00	0.065	40.00	75.74	75.78

present research, five levels were applied for four parameters including pH, contact time, initial dye concentration and adsorbent dosage. The content and levels of the four mentioned independent parameters with real and coded amounts of each parameter have been listed in Table I. Two levels; low (-1) and high (+1) were coded for the independent parameters, in which the axial points are coded as -2 and +2. A five-level-four-factors full fraction central composite design was applied to build a second-order response surface model using 30 randomly runs and the percentage of removal for each runs was calculated. The complete CCD design matrix as an actual independent parameter is applied and the obtained result is presented in Table I. To reduce the rate of errors, the experiments were repeated several times. The model of the adsorption process is explained by the following quadratic equation [34]:

$$y = \beta_0 + \sum_{i=1}^{k} \beta_i X_i + \sum_{i=1}^{k} \beta_{ii} X_i^2 + \sum_{i=1}^{k} \sum_{j=1}^{k} \beta_{ij} X_i X_j + \varepsilon \quad (3)$$

Where Y is the predicted response function (% Removal), β_0 and ε are constant and error terms respectively, X_i and X_j are the coded values of our independent parameters, β_i is the linear coefficient, β_{ii} is the quadratic coefficient and β_{ij} is the interaction coefficient.

The collected number of 30 runs were applied to find mathematical correlate among the independent parameters and the corresponding response values. Results were analyzed by using the analysis of variance (ANOVA) and the validity of the response surface model was investigated by measuring the regression coefficients (R^2) and the lack of fit (LOF) of the model. Moreover, the most effective factors were determined on the basis of F- values and P- values (confidence surface= 0.95). In addition, by plotting the three-dimensional plots of response (% Removal) vs. significant parameters using Design-Expert 7 software, the best condition of dye adsorption was found graphically [35].

RESULTS AND DISCUSSION

Characterization of MOF

The FT-IR spectrum of the Ni-MOF and 4, 4′-diaminodiphenyl sulfone (DAP) ligand are

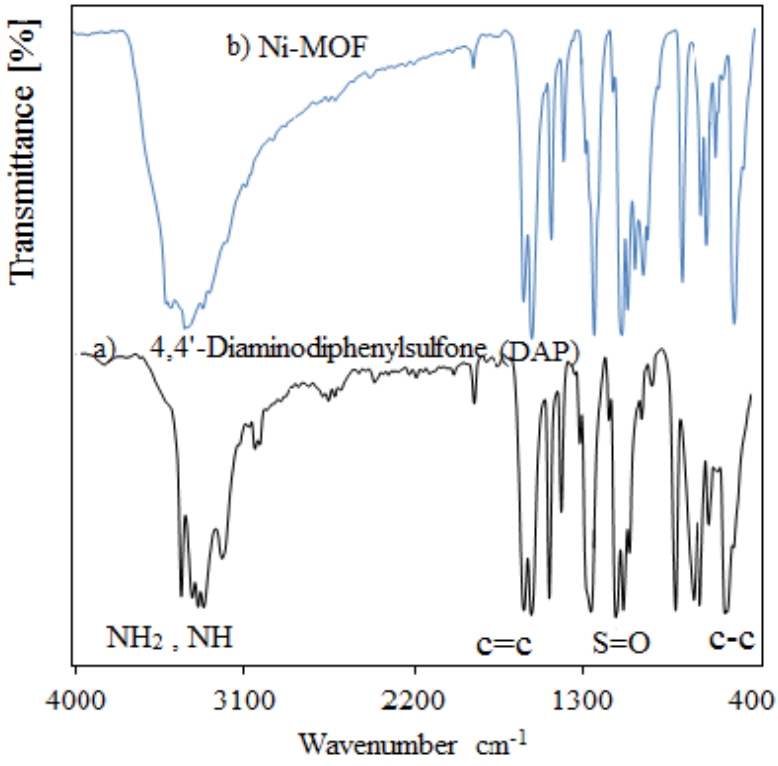

Fig. 1. FT-IR spectra of (a) DAP, (b)Ni-MOF

illustrated in Fig. 1. The FT-IR of DAP spectrum (Fig. 1a) shown a band within the range of 3454-3238 cm^{-1} and a band in 1587 cm^{-1} correspond to symmetric and asymmetric stretching vibration of NH_2 and NH and bending mode of NH. The bands observed at 1145-1277 cm^{-1} corresponds to both symmetric and asymmetric style of SO_2 stretching fluctuation and the S=O bending fluctuation at 554 cm^{-1}. The bands appearing at 1495-1632 and 3235 cm^{-1} are corresponded to the aromatic C=C group and to stretching fluctuation of aromatic C-H, respectively. The observed peak at 1075 and 1586 are assigned to C-N stretching and N-H bending vibrations, respectively. Fig. 1b shows the FT-IR spectrum of the Ni-MOF demonstrating bands at 3313,3471,3243,3442 cm^{-1} from N-H groups, 1133 and 1282 cm^{-1} stretching vibrations and, 544 cm^{-1}bending vibration from SO_2 group,1631 and 1492 the aromatic C=C group,1075 and 1595 cm^{-1} corresponded to C-N and bending fluctuation of N-H , respectively. The mass of the bands of Ni-MOF and DAP were nearly matching although, stretching and bending vibrations were shifted.

Fig. 2 displays the pattern of X-ray diffraction of Ni-MOF and DAP ligand. The peaks appeared in diffractogram of Ni-MOF are in agreement with DAP and Ni patterns with orthorhombic crystal system (JCPDS card no. 00-040-1928) and cubic structure (JCPDS card no. 01-089-2810), respectively. The XRD pattern of Ni-MOF (Fig. 2b) shows distinct crystalline peaks around at 2θ= 45° and 51.25° respectively related to (111) and (200)) crystalline planes and clearly have been revealed the presence of Ni in Ni-MOF [36]

The surface morphology of synthesized Ni-MOF was characterized by FESEM microscope(Fig. 3). The image of FESEM represents a superficial area with slightly ordered and porous structure that confirms highly uniform distribution of Ni-MOF. The EDX spectrum of sample is also given in Fig. 3. The presence of Carbon, Sulfur, Oxygen, Nitrogen, and Nickel peaks in spectrum indicates the incorporation of these elements in sample.

Values of the surface area, mean pore diameter

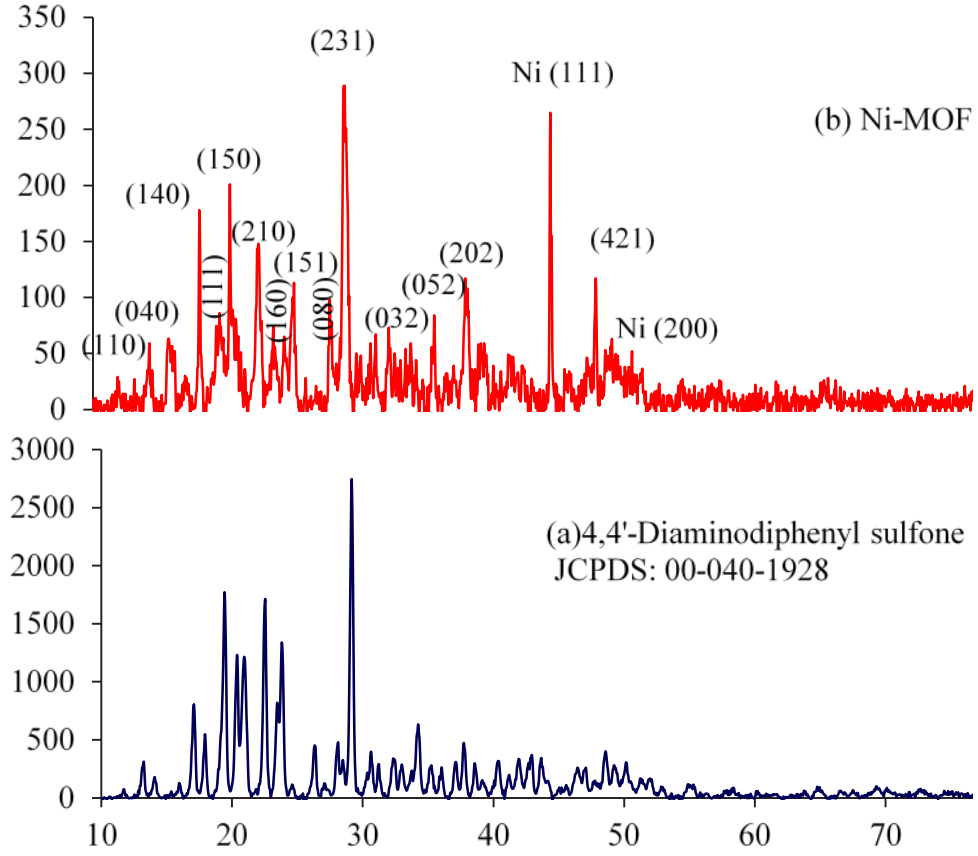

Fig. 2. XRD pattern of (a) DAP, (b)Ni-MOF

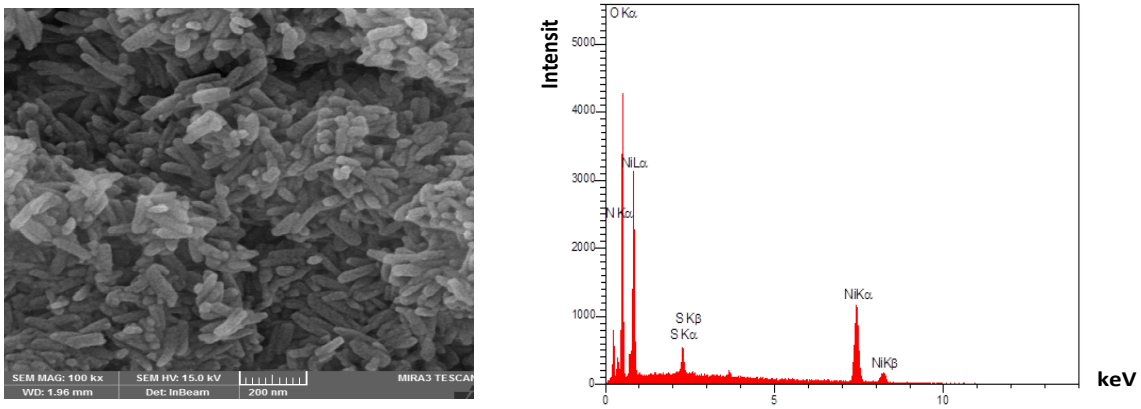

Fig. 3. FESEM image and EDX spectra of Ni-MoF

and total pore volume at P/P_0 = 0.99 of Ni-MOF was achived using physical adsorption-desorption of Nitrogen gas 6.669 m^3/g, 22.646 nm and 0.038 cm^3/g respectively (Fig. 4). The shape of hysteresis loop in Fig. 4 implies that the Ni-MOF structure is exhibited type IV of isotherm which is characteristic of mesoporous solids according to IUPAC classification.

Thermogravimetric and differential gravimetric analysis (TGA/DTG) results of synthesized Ni-MOF has been shown in Fig. 5. TGA uses a thermobalance to estimate the relationship between mass and the temperature in the range of 25 - 800°C under argon flow with the slope of 20°C per minute. According to the TG curve, 3.65% initial weight loss has happened in the temperature range of 31.98 - 123.45 ˚C because of water evaporation for adsorbed foreign molecules and after that, the amount of weight has almost reached a stable state. Until at 367° C, pyrolysis of the organic moiety causes a %46 reduction in the weight of Ni-MOF. Therefore, it can be concluded that there is thermal stability for Ni-MOF at temperatures less than 360° C.

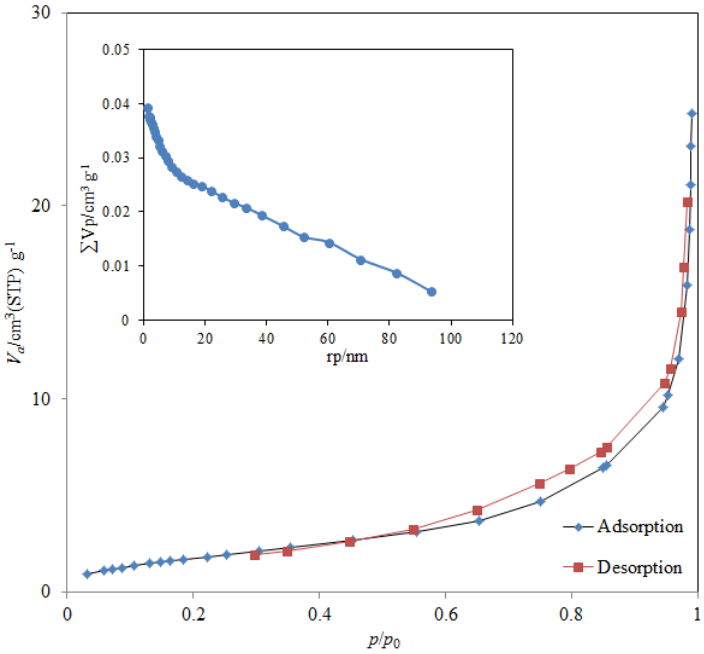

Fig. 4. BJH method (inset)of Ni-MOF for evaluation of N2 adsorption–desorption isotherm and pore size distribution

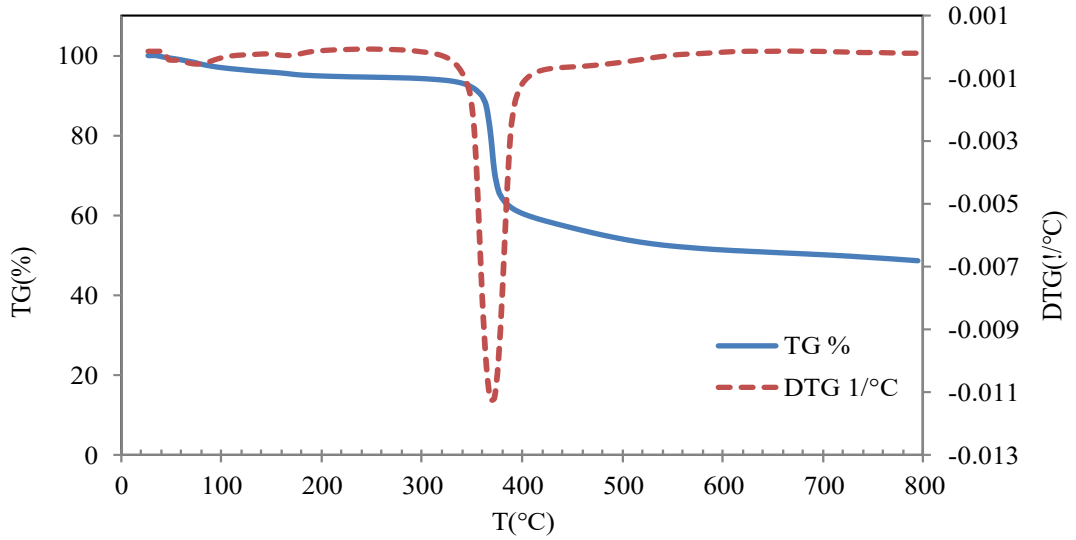

Fig. 5. DTG-TG thermogram of Ni-MOF

Central composite design

As previously described in this study, CCD method was used to investigate the effect of four factors: pH, contact time, adsorbent dosage and RB concentration (Table 1) to remove RB and determine the necessary conditions for optimizing the results.

Analysis of variance (ANOVA) was administered to evaluate the removal percentage of the RB dye (Table 2). The F-test was performed for finding the validity of the polynomial model equation based on the coefficient of determination (R^2) and statistical significance of the equation. P-values <0.05 is considered as the significance of each term, at 95% confidence level. In this way, the model was able to predict and determine the removal percentage of RB dye in terms of important parameters.

Eq. (4) illustrates the relation between removal percentage (%R) and the actual independent parameters:

$$\begin{aligned} Y\ (\%R) &= 90.26 + 16.38A - 1.99B \\ &+2.19C + 9.65D + 0.61AB \\ &-1.99AC - 5.05AD + 2.81BC \\ &+1.86BD + 2.63CD - 10.82A^2 \\ &-0.92\ B^2 - 1.42C^2 - 4.40D^2 \end{aligned} \quad (4)$$

The positive and negative coefficients determine that their corresponding terms positively or negatively are influence the response.

Fisher's F test in the ANOVA was used for statistical evaluation of the designed model. The ANOVA results for removal percentage are illustrated in Table 2. The lower probability (P-value < 0.0001) is an indicator of significant and reliable model at the 5% confidence level where the lack of fit (LOF) of model is not significant relative to the prime error. The coefficients of determination (R^2), the adjusted coefficients of determination (R^2_{adj}) and the predicted coefficients of determination (R^2_{pred}) of the model for the response surface regression have been obtained 0.9998, 0.9976 and 0.9936, respectively that confirms the accuracy and validity of the quadratic model. The adequate precision (Adeq Precision=116.116) is the indicator of signal-to-noise ratio a ratio greater than 4 is ideal and showing the adequate signal for model could be utilize negative the design space.

Table 2 also indicates the linear coefficients (A, B, C and D), interactive factors coefficient (AB, AD, BC, and BD) and quadratic term (A^2, B^2, C^2, and D^2) significantly improved the efficiency of RB removal by Ni (II)- MOF (P < 0.05).

Three-dimensional response surface plot

Three-dimensional response surface, is a graphical tool for illustration of the interaction effects, using plotting the response versus two independent factors (keeping the other parameters at a fixed level) [2, 3]. The obtained response surface plots of independent parameters accounts as a predictor of the removal percentage

Table 2. Analysis of variance (ANOVA) of the fitted quadratic equations for dyes adsorption for RB (%R) by Ni(II)- MOF.

Source	SS[a]	Df[b]	MS[c]	F-value	p-Value	Remark
Model	13122.37	14	937.31	862.95	< 0.0001	mostly significant
A	6437.25	1	6437.25	5926.57	< 0.0001	mostly significant
B	95.22	1	95.22	87.66	< 0.0001	mostly significant
C	115.52	1	115.52	106.36	< 0.0001	mostly significant
D	2236.69	1	2236.69	2059.25	< 0.0001	mostly significant
AB	6.05	1	6.05	5.57	0.0323	
AC	63.21	1	63.21	58.20	< 0.0001	
AD	408.54	1	408.54	376.13	< 0.0001	
BC	126.13	1	126.13	116.13	< 0.0001	
BD	55.62	1	55.62	51.21	< 0.0001	
CD	110.87	1	110.87	102.08	< 0.0001	
A^2	3208.28	1	3208.28	2953.76	< 0.0001	
B^2	23.22	1	23.22	21.38	0.0003	
C^2	55.67	1	55.67	51.25	< 0.0001	
D^2	530.23	1	530.23	488.17	< 0.0001	
Residual	16.29	13	1.09	2.92		
Lack of Fit	13.91	10	1.39	862.95	0.1241	Not significant
Pure Error	2.38	3	0.48			
Cor Total	13138.67	29				

R^2= 0.9988, Adj R^2= 0.9976, Pred R^2= 0.9936

[a]Sum of square, [b]Degree of freedom, [c]Mean square.

at other conditions. The 3D response surface plots have been illustrated in Fig. 6a–c.

In Fig. 6a, the influence of adsorbent mass and pH on removal percentage is illustrated at a RB concentration of 14.39 mg/L and 37.30 min of contact time. When adsorbent mass increased from 0.035 to 0.065 and pH increased from 5.0 to 9.0, the removal percentage is increased. This is due to increment of the contact surface area and exchangeable sites. Fig. 6b shows the effect of pH and initial RB concentration on the removal percentage.

Finally, It can be found from Fig. 6c, increasing of contact time and adsorbent mass affect positively on the removal percentage, enhancement of the adsorbent mass led to unsaturated adsorbent sites to keep the initial RB concentration and pH at constant level. A maximum removal percentage of 99.13 was obtained at pH 8.5 and 14.39 mg/L of RB concentration. Increment of the removal percentage mostly observed at the pH 8.5 because of cationic nature of the RB. The excess amount of H^+ ions at acidic condition, decrease the amount of negatively charged adsorbent positions, while increase the amount of positively charged surface positions probably is not ideal for the adsorption of cationic dye [37]. Thus, higher pH and excessive negative charged surface on the Ni (II)- MOF adsorbent, increase the adsorption of cationic RB ions.

In fact, the maximum removal percentage of RB (99.13%) was obtained at these following conditions: pH of 8.5, an RB concentration of 14.39 mg/L, an adsorbent dosage of 0.057 g and time of 37.30 min.

Perturbation plot illustrates the positive effect of factors on the efficiency of the removal. As observed at perturbation plot presented in Fig. 7, all mentioned factors had a significant effect on the efficiency of removal. Enhancement of PH, contact time, and adsorbent dosage, improve the removal efficiency. However, increment in RB concentration contributes to decreased it. It can be concluded that pH and RB concentration had a main effect on the removal efficiency.

As illustrated in the Box-Cox normality plot (Fig. 7), the lowest point on the plot that indicates the lambda's best value is (1), as a result, the transformation of the removal percentage response was unnecessary.

Adsorption isotherm study

Adsorption isotherms study is important for gattering properties and mechanism of adsorption. The adsorption isotherms indicate the amount of adsorbate molecules from the solid sorbent and the liquid sample solution in the adsorption process. So, to determine the adsorption isotherm of the process, the general isotherms like Langmuir and Freundlich were investigated at different concentrations in the range of (5-40) mg/L in optimum conditions. Langmuir isotherm model

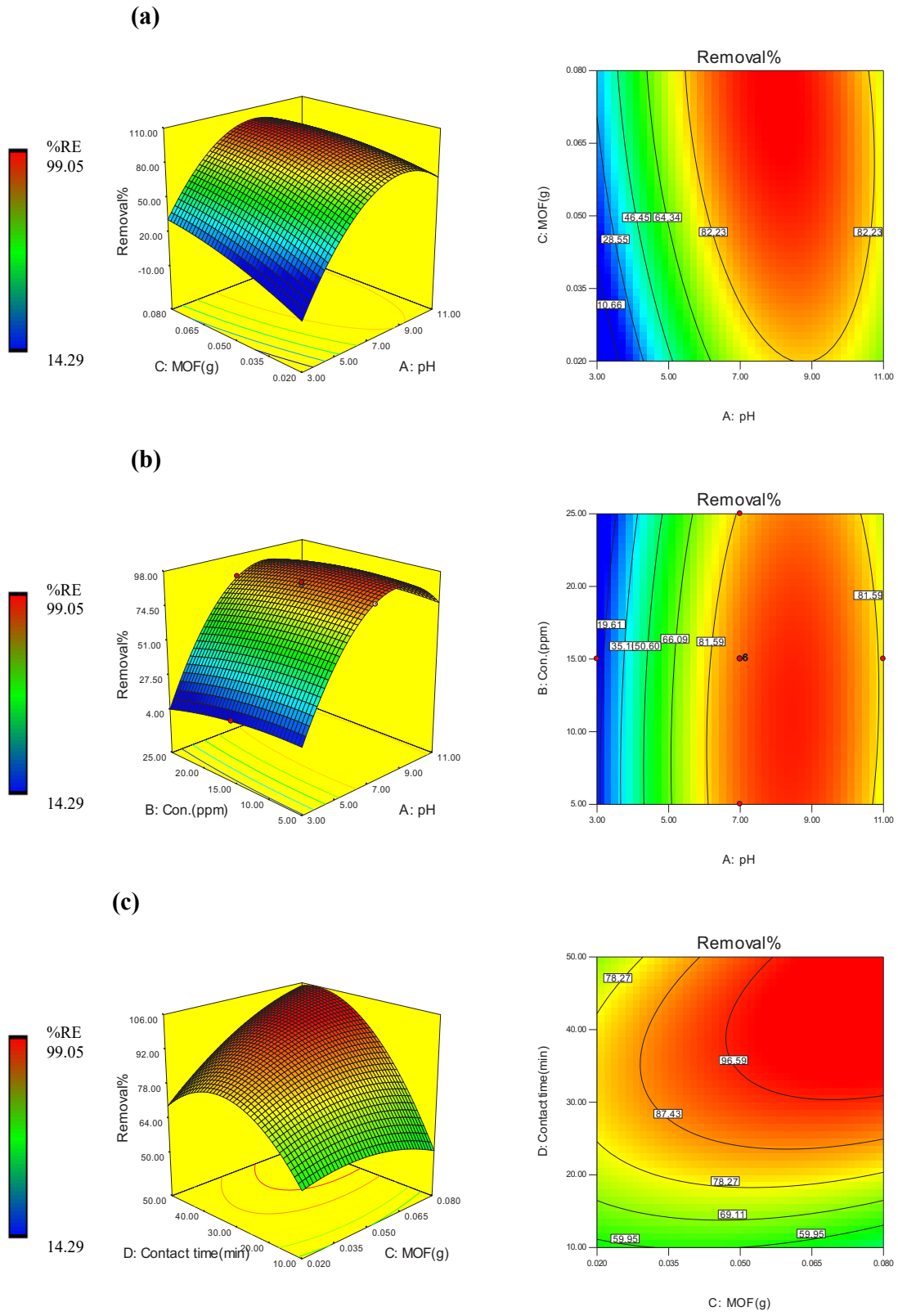

Fig. 6. Response surface plots for interactive effect of (a) pH and adsorbent dosage (b) pH and RB concentration (c) adsorbent dosage and contact time on removal percentage.

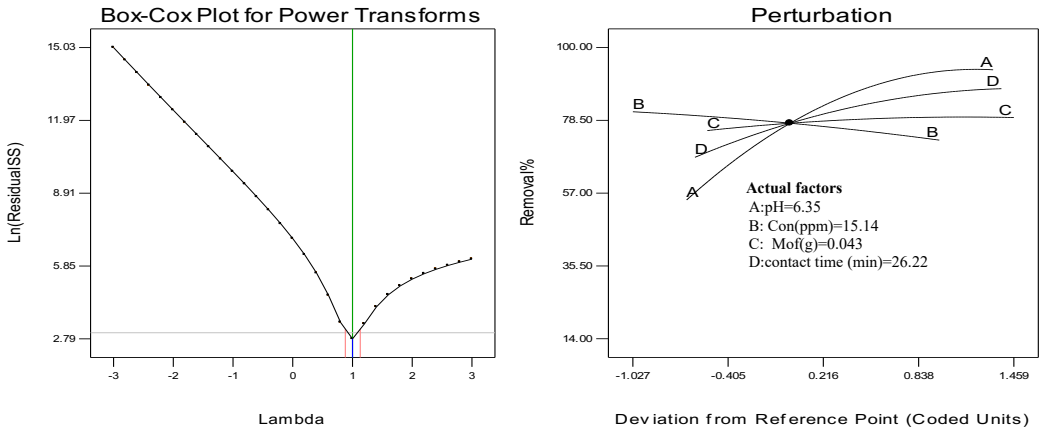

Fig.7 Box- Cox plot and perturbation plots for RB removal percentage by Ni-MOF.

hyphothesis is based on the fact that the intraction between molecules is in the form of monolayer adsorption. According to this, the linearized form of Langmuir isotherm model is as below [38]:

$$\frac{C_e}{q_e} = \frac{1}{K_L q_m} + \frac{C_e}{q_m} \quad (5)$$

$$R_L = \frac{1}{1 + K_L C_0} \quad (6)$$

Where C_e is the equilibrium concentration of the RB solution (mg/L), q_m and q_e are adsorption capacity of dye (mg/g) at time t and the equilibrium state, respectively and K_L is the Langmuir constant of adsorption.

The plot of C_e/q_e versus C_e, leading to a linear line for RB. K_L and q_m were got from slope and the intercept of the plots. R_L (separation factor) is indictor of desired RB adsorption onto Ni (II)- MOF.

The R_L is the attainable, (R_L=1) is linear, (0<R_L<1) is ideal, and(R_L=0) is irreversible kind of adsorption process [39]. According to the Table 4, the value of R_L for RB dye is 0.0923 that showed that the adsorption of RB by Ni (II)-MOF adsorbent was ideal.

The Freundlich isotherm is utilized for many adsorption processes. In this study, the Freundlich isotherm was also investigated for the process. The equation is as following:

$$q_e = K_f C_e^{\frac{1}{n}} \quad (7)$$

The linearized form of the Freundlich isotherm can be as below:

$$\ln q_e = \ln K_F + \frac{1}{n} \ln C_e \quad (8)$$

Where C_e, K_f, and 1/n are the equilibrium concentration of the RB (mg/L), the Freundlich constant [(mg/g)(L/mg)$^{1/n}$] and heterogeneity

Table 3. Constants of the Isotherm models calculated for the adsorption of RB by Ni (II)- MOF.

Model	Parameters	Value
Langmuir	q_{max}(mg g^{-1})	163.93
	K_L (L mg^{-1})	0.0727
	R_L	0.0340
	R^2	0.9827
Freundlich	1/ n	0.5695
	K_f (mg g^{-1})(L mg^{-1})$^{1/n}$	14.0679
	R^2	0.9760

Table 4. Constants of the Kinetic models described of RB adsorption on the Ni(II)-MOF.

Model	Parameters	Value
Pseudo-first-order	$k_1(min^{-1})$	0.0680
	q_e(calc)(mg g^{-1})	10.8843
	R^2	0.9117
Pseudo-second-order	k_2(g mg^{-1} min^{-1})	0.0094
	q_e(calc)(mg g^{-1})	20.7468
	R^2	0.9927
	qe (exp) (mg g^{-1})	19.6340

factor that shows the adsorption intensity, respectively.

The values of 1/n and K_f were achived from the slope and the intercept of the linear plot of ln versus ln.

The value of 1/n in the range of (0-1) indicates the heterogenity of surface [40, 41]. As can be seen in Table 3, the value of 1/n in this study was 0.5695 that shows an ideal RB dye adsorption on hetergenous surface.

Adsorption kinetics

Pseudo-first-order and pseudo-second-order models was applied for kinetic adsorption modeling. The kinetic of RB adsorption on the Ni(II)- MOF was investigated in the pseudo-first-order (Eq. 9) and pseudo-second-order (Eq. 10) models [42], respectively.

$$\log(q_e - q_t) = \log(q_e) - \frac{K_1}{2.303}t \quad (9)$$

$$\left(\frac{t}{q_t}\right) = \frac{1}{K_2\, q_e^2} + \frac{1}{q_e}t \quad (10)$$

q_e and q_t = adsorbed RB at equilibrium time (mg/g)

K_1 (1/min) and K_2 (g/mg min) = the adsorption rate constant calculated by slopes pf both lines. while the intercept of lines are utilized to calculate experimental adsorption capacity [43, 44].

As observed in Table 3, the closeness of theoretical and experimental adsorption capacity is obtained in pseudo-second-order kinetic model. The higher correlation coefficient value of adsorption step indicates the ideality of this model for experimental data studying.

Regeneration study

The regeneration of Ni-MOF as a key factor for the cost-effective removal of RB from aqueous solutions was checked by adsorption and desorption of RB onto Ni-MOF. Hence, ethanol, methanol, and a mixture of ethanol and methanol (1:1, v/v) solutions were used for desorbing of RB dye to perform regeneration. The maximum desorption was obtained in pure methanol. Successive exploiting of adsorbent (0.057 g) at optimum conditions and it regenerated at eight cycles following successive exploiting (Fig. 8). Eight consecutive cycles of absorption and excretion were performed so that up to the fourth form of absorption is above 90%. The desorption of Ni-MOF was also good up to the fourth form of absorption with more than 90% and further consumption gradually devaluation to value less than 50% for RB.

Table 5. Properties of different MOFs for dye removal in term of temperature, contact time, sorption capacity

Adsorbent	Temperature (˚C)	Contact time (min)	Sorption capacity (mg g^{-1})	Ref.
Fe_3O_4/MIL-100(Fe)	ambient	90	28.36	[45]
Kaolinite	30	80	46.08	[46]
Sodium montmorillonite	40	1440	42.19	[1]
HKUST-1 MOF	ambient	4	38.80	[47]
activated carbon-HKUST-1-MOF	ambient	4	65.37	[[47]
CZIF-867	70	300	116.2	[48]
Eichhornia Crassipes powder	ambient	30	44.60	[49]
Ni-Mof	ambient	39	163.66 3	This work

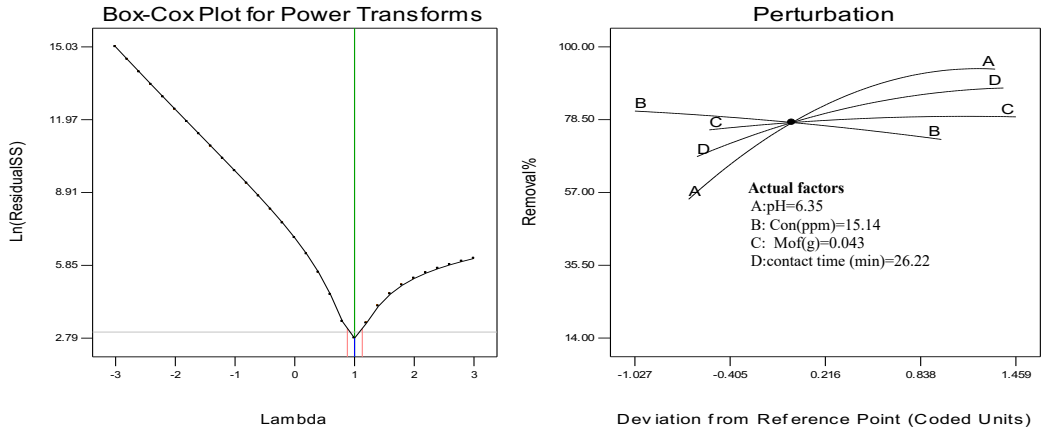

Fig. 8. Regenerate and exploit of Ni-MOF of RB dye by absolute methanol solvent. mean ± SD is applied for each 5 sample.

The maximum monolayer adsorption capacities (values of q_m), contact time and Temperature for the dye removal different adsorbents are listed in Table 5. Since the experiments were performed under different conditions, comparing their results with each other is not very correct but according to the obtained results, the performance of Ni-MOF for RB removal is suitable.

CONCLUSION

The Ni (II)- MOF, was synthesized and characterized using FT-IR, FESEM, EDX and XRD analysis and applied for RB dye removal from aqueous solutions. The optimum conditions for obtaining the higher dye removal (99.13%) were achieved in the following condition: pH of 8.50, contact time of 37.30 min for initial concentration of the RB =14.39 ppm and adsorbent mass = 0.057 g. The CCD as a statistical model, was applied for optimization of variable. The adsorption process was studied using Pseudo-order and Pseudo-second-order. Langmuir model was indicator of RB adsorption onto the adsorbent according to Pseudo-second-order model.

CONFLICT OF INTEREST

The authors declare that there is no conflict of interests regarding the publication of this manuscript.

REFERENCES

1. Selvam PP, Preethi S, Basakaralingam P, N.Thinakaran, Sivasamy A, Sivanesan S. Removal of rhodamine B from aqueous solution by adsorption onto sodium montmorillonite. J Hazard Mater. 2008;155(1-2):39-44.
2. Yu W, Luo M, Yang Y, Wu H, Huang W, Zeng K, Luo F. Metal-organic framework (MOF) showing both ultrahigh As(V) and As(III) removal from aqueous solution. J Solid State Chem. 2019;269:264-70.
3. Asheghhosseini A, Zolgharnein J. Iron terephthalate metal–organic framework (MOF-235) as an efficient adsorbent for removal of toluidine blue dye from aqueous solution using Box–Behnken design as multivariate optimization approach. Journal of the Iranian Chemical Society. 2020;17(10):2663-73.
4. Xu D, Ma H. Degradation of rhodamine B in water by ultrasound-assisted TiO_2 photocatalysis. Journal of Cleaner Production. 2021;313:127758.
5. Mohammadi M, Hassani AJ, Mohamed AR, Najafpour GD. Removal of Rhodamine B from Aqueous Solution Using Palm Shell-Based Activated Carbon: Adsorption and Kinetic Studies. Journal of Chemical & Engineering Data. 2010;55(12):5777-85.
6. Vidal J, Villegas L, Peralta-Hernández JM, Salazar González R. Removal of Acid Black 194 dye from water by electrocoagulation with aluminum anode. Journal of Environmental Science and Health, Part A. 2016;51(4):289-96.
7. Tian Y, Ju B, Zhang S, Hou L. Thermoresponsive cellulose ether and its flocculation behavior for organic dye removal. Carbohydr Polym. 2016;136:1209-17.
8. Serpone N, Horikoshi S, Emeline AV. Microwaves in advanced oxidation processes for environmental applications. A brief review. Journal of Photochemistry and Photobiology C: Photochemistry Reviews. 2010;11(2-3):114-31.
9. Li C, Cui J, Wang F, Peng W, He Y. Adsorption removal of Congo red by epichlorohydrin-modified cross-linked chitosan adsorbent. Desalination and Water Treatment. 2015;57(30):14060-66.
10. Konicki W, Hełminiak A, Arabczyk W, Mijowska E. Removal of anionic dyes using magnetic Fe@graphite core-shell nanocomposite as an adsorbent from aqueous solutions. Journal of Colloid and Interface Science. 2017;497:155-64.
11. Qiu J, Feng Y, Zhang X, Jia M, Yao J. Acid-promoted synthesis of UiO-66 for highly selective adsorption of anionic dyes: Adsorption performance and mechanisms. Journal of Colloid and Interface Science. 2017;499:151-58.
12. Jain R, Mathur M, Sikarwar S, Mittal A. Removal of the hazardous dye rhodamine B through photocatalytic and adsorption treatments. J Environ Manage. 2007;85(4):956-

64.
13. Gupta VK, Ali I. Water Treatment: Low-Cost Alternatives to Carbon Adsorbents. Encyclopedia of Surface and Colloid Science, Third Edition: Taylor & Francis; 2015. p. 7618-52.
14. Aprea P, Caputo D, Gargiulo N, Iucolano F, Pepe F. Modeling Carbon Dioxide Adsorption on Microporous Substrates: Comparison between Cu-BTC Metal–Organic Framework and 13X Zeolitic Molecular Sieve. Journal of Chemical & Engineering Data. 2010;55(9):3655-61.
15. Guo R, Guo J, Yu F, Gang DD. Synthesis and surface functional group modifications of ordered mesoporous carbons for resorcinol removal. Microporous Mesoporous Mater. 2013;175:141-46.
16. Haque E, Jun JW, Jhung SH. Adsorptive removal of methyl orange and methylene blue from aqueous solution with a metal-organic framework material, iron terephthalate (MOF-235). J Hazard Mater. 2011;185(1):507-11.
17. Liu K, Li H, Wang Y, Gou X, Duan Y. Adsorption and removal of rhodamine B from aqueous solution by tannic acid functionalized graphene. Colloids Surf Physicochem Eng Aspects. 2015;477:35-41.
18. Férey G. Hybrid porous solids: past, present, future. Chem Soc Rev. 2008;37(1):191-214.
19. Kitagawa S, Kitaura R, Noro Si. Functional Porous Coordination Polymers. Angew Chem Int Ed. 2004;43(18):2334-75.
20. Yaghi OM, O'Keeffe M, Ockwig NW, Chae HK, Eddaoudi M, Kim J. Reticular synthesis and the design of new materials. Nature. 2003;423(6941):705-14.
21. Murray LJ, Dincă M, Long JR. Hydrogen storage in metal–organic frameworks. Chem Soc Rev. 2009;38(5):1294.
22. Farrusseng D, Aguado S, Pinel C. Metal–Organic Frameworks: Opportunities for Catalysis. Angew Chem Int Ed. 2009;48(41):7502-13.
23. Li J-R, Kuppler RJ, Zhou H-C. Selective gas adsorption and separation in metal–organic frameworks. Chem Soc Rev. 2009;38(5):1477.
24. Horcajada P, Serre C, Maurin G, Ramsahye NA, Balas F, Vallet-Regí M, et al. Flexible Porous Metal-Organic Frameworks for a Controlled Drug Delivery. Journal of the American Chemical Society. 2008;130(21):6774-80.
25. Hasan Z, Jhung SH. Removal of hazardous organics from water using metal-organic frameworks (MOFs): Plausible mechanisms for selective adsorptions. J Hazard Mater. 2015;283:329-39.
26. Wang H, Yuan X, Wu Y, Zeng G, Chen X, Leng L, Li H. Synthesis and applications of novel graphitic carbon nitride/metal-organic frameworks mesoporous photocatalyst for dyes removal. Applied Catalysis B: Environmental. 2015;174-175:445-54.
27. Wang C-C, Li J-R, Lv X-L, Zhang Y-Q, Guo G. Photocatalytic organic pollutants degradation in metal–organic frameworks. Energy Environ Sci. 2014;7(9):2831-67.
28. Witek-Krowiak A, Chojnacka K, Podstawczyk D, Dawiec A, Bubała K. Application of response surface methodology and artificial neural network methods in modelling and optimization of biosorption process. Bioresour Technol. 2014;160:150-60.
29. Dil EA, Ghaedi M, Asfaram A, Mehrabi F, Bazrafshan AA, Ghaedi AM. Trace determination of safranin O dye using ultrasound assisted dispersive solid-phase micro extraction: Artificial neural network-genetic algorithm and response surface methodology. Ultrason Sonochem. 2016;33:129-40.
30. Janani M, Senejani MA, Isfahani TM. An Efficient Synthesis of Benzimidazole and Benzothiazole Derivatives Using a Nickel(II) Metal-Organic Framework. Current Organic Synthesis. 2020;17(2):109-16.
31. Dey C, Kundu T, Biswal BP, Mallick A, Banerjee R. ChemInform Abstract: Crystalline Metal-Organic Frameworks (MOFs): Synthesis, Structure and Function. ChemInform. 2014;45(26).
32. Gao X-Z, Liu H-J, Cheng F, Chen Y. Thermoresponsive polyaniline nanoparticles: Preparation, characterization, and their potential application in waterborne anticorrosion coatings. Chem Eng J. 2016;283:682-91.
33. Dil EA, Ghaedi M, Ghaedi A, Asfaram A, Jamshidi M, Purkait MK. Application of artificial neural network and response surface methodology for the removal of crystal violet by zinc oxide nanorods loaded on activate carbon: kinetics and equilibrium study. Journal of the Taiwan Institute of Chemical Engineers. 2016;59:210-20.
34. Asfaram A, Ghaedi M, Goudarzi A, Rajabi M. Response surface methodology approach for optimization of simultaneous dye and metal ion ultrasound-assisted adsorption onto Mn doped Fe_3O_4-NPs loaded on AC: kinetic and isothermal studies. Dalton Transactions. 2015;44(33):14707-23.
35. Ghaedi M, Khafri HZ, Asfaram A, Goudarzi A. Response surface methodology approach for optimization of adsorption of Janus Green B from aqueous solution onto ZnO/$Zn(OH)_2$-NP-AC: Kinetic and isotherm study. Spectrochimica Acta Part A: Molecular and Biomolecular Spectroscopy. 2016;152:233-40.
36. Nayak BB, Vitta S, Nigam AK, Bahadur D. Ni and Ni–nickel oxide nanoparticles with different shapes and a core–shell structure. Thin Solid Films. 2006;505(1-2):109-12.
37. Mohanty K, Naidu JT, Meikap BC, Biswas MN. Removal of Crystal Violet from Wastewater by Activated Carbons Prepared from Rice Husk. Industrial & Engineering Chemistry Research. 2006;45(14):5165-71.
38. Muthukumaran C, Sivakumar VM, Thirumarimurugan M. Adsorption isotherms and kinetic studies of crystal violet dye removal from aqueous solution using surfactant modified magnetic nanoadsorbent. Journal of the Taiwan Institute of Chemical Engineers. 2016;63:354-62.
39. Nassar MY, Ahmed IS, Mohamed TY, Khatab M. A controlled, template-free, and hydrothermal synthesis route to sphere-like α-Fe_2O_3 nanostructures for textile dye removal. RSC Advances. 2016;6(24):20001-13.
40. Teimouri A, Nasab SG, Vahdatpoor N, Habibollahi S, Salavati H, Chermahini AN. Chitosan /Zeolite Y/Nano ZrO_2 nanocomposite as an adsorbent for the removal of nitrate from the aqueous solution. Int J Biol Macromol. 2016;93:254-66.
41. Mohamad Aizad Mohd M, Roshafima Rasit A, Eleen Dayana Mohamed I. Silver Nanoparticles Loaded Activated Carbon Synthesis Using Clitorea Ternatea Extract for Crystal Violet Dye Removal. Journal of Research in Nanoscience and Nanotechnology. 2021;3(1):26-36.
42. Labidi A, Salaberria AM, Fernandes SCM, Labidi J, Abderrabba M. Adsorption of copper on chitin-based materials: Kinetic and thermodynamic studies. Journal of the Taiwan Institute of Chemical Engineers. 2016;65:140-48.
43. Wu F-C, Tseng R-L, Juang R-S. Kinetic modeling of liquid-

phase adsorption of reactive dyes and metal ions on chitosan. Water Res. 2001;35(3):613-18.
44. Ho YS, McKay G. Pseudo-second order model for sorption processes. Process Biochem. 1999;34(5):451-65.
45. Liu H, Ren X, Chen L. Synthesis and characterization of magnetic metal–organic framework for the adsorptive removal of Rhodamine B from aqueous solution. Journal of Industrial and Engineering Chemistry. 2016;34:278-85.
46. Khan TA, Dahiya S, Ali I. Use of kaolinite as adsorbent: Equilibrium, dynamics and thermodynamic studies on the adsorption of Rhodamine B from aqueous solution. Applied Clay Science. 2012;69:58-66.
47. Azad FN, Ghaedi M, Dashtian K, Hajati S, Pezeshkpour V. Ultrasonically assisted hydrothermal synthesis of activated carbon–HKUST-1-MOF hybrid for efficient simultaneous ultrasound-assisted removal of ternary organic dyes and antibacterial investigation: Taguchi optimization. Ultrason Sonochem. 2016;31:383-93.
48. Zhang J, Yan X, Hu X, Feng R, Zhou M. Direct carbonization of Zn/Co zeolitic imidazolate frameworks for efficient adsorption of Rhodamine B. Chem Eng J. 2018;347:640-47.
49. Saufi H, Alouani MEL, Aride J, Taibi Mh. Rhodamine B biosorption from aqueous solution using Eichhornia crassipes powders: Isotherm, kinetic and thermodynamic studies. Chemical Data Collections. 2020;25:100330.